Journal of Archaeological Science (1996) **23,** 419–428

Calibration and Visualization of Wall-Thickness and Porosity Distributions of Ceramics Using X-radiography and Image Processing

A. Pierret

Institut National Agronomique, Science du Sol et Hydrologie, Thiverval-Grignon 78850 France

C. J. Moran

Commonwealth Scientific and Industrial Research Organization, Division of Soils, GPO Box 639, ACT 2601, Australia

L.-M. Bresson

Institut National Agronomique, Science du Sol et Hydrologie, Thiverval-Grignon 78850, France

(*Received 26 October 1994, revised manuscript accepted 11 April 1995*)

It has been reported that X-radiography studies of archaeological ceramics can be used to identify fashioning processes. However, diagnostic criteria used for such interpretations often appear unconvincing to the non-specialist. The qualitative nature of the interpretations is a significant factor in this quality assessment. Published reproductions of X-radiographs rarely clearly demonstrate the structural patterns observed and described. It is possible to describe quantitatively features in X-radiographs that are indicative of particular fashioning techniques. Unfortunately, this usually requires access to digital X-ray equipment. A method is described here for acquiring and calibrating digital images from X-radiographs exposed onto standard film. Often with ceramics, thickness and density information are confounded in X-radiographs. A low-pass filtering technique is used to remove the density information. The resulting image is then calibrated using Lambert's Law of X-ray absorbtion combined with some simple measurements to produce a sherd thickness map. The filtered density information is then similarly treated to drive a density distribution across the sherd. The use of the technique is illustrated on three specimens from an experiment in which the fashioning techniques were carefully controlled. Enhanced images are used to document features which distinguish the three fashioning techniques. Measurement of such features and quantitative interpretation of wall thickness of ceramics are highlighted as research areas which require further attention.

Keywords: CERAMIC TECHNOLOGY, RADIOGRAPHY, IMAGE PROCESSING, WALL-THICKNESS, POROSITY DISTRIBUTION, MATHEMATICAL MORPHOLOGY.

Introduction

The identification of fashioning techniques is now an important topic in archaeological ceramic studies. Initially, determinations were based on simple criteria related to the surface texture of sherds. Repeated observations in ethnographic and experimental situations (van der Leeuw, 1976; Rye, 1977, 1981; Balfet, 1984; Rice, 1987: 141), indicated that superficial attributes were problematic because they often result from the last steps of the forming process, e.g. surface finishing. It has been proposed that characteristic surface attributes should be scrutinized in parts of vessels usually hidden from view, i.e. the interior of closed shapes and the exterior of open ones (van der Leeuw, 1976: 240; Rye, 1977: 205; van As, 1984: 140) because potters rarely remove the original traces of the forming operations. Despite surface features being of use to suggest possible recurrent patterns of fashioning (Vandiver, Ellingson, Robinson, Lobick & Séguin, 1991: 186), they are often ambiguous and unevenly expressed from one sherd to another (Courty & Roux, 1995). Thus, surface features constitute indications rather than indisputable results and require confirmation with supporting evidence. Consequently, it has been suggested that the internal structure of sherds may provide such data. The organization of temper particles and voids should reflect specific deformations corresponding to different primary forming forces (Shepard, 1956; Bordet &

0305-4403/96/030419+10 $18.00/0

Courtois, 1967; Rye, 1977, 1981; Woods, 1985). Optical and electron microscopy have been tested for this purpose but their usefulness appears to depend on the materials studied (Vandiver, 1987; Pierret, 1994; Courty & Roux, 1995).

X-ray imaging has been demonstrated to provide valuable qualitative data for documenting fashioning procedures (e.g. see Rye, 1977, 1981; Vandiver, 1987; McGovern, 1989; Carr, 1990; Vandiver *et al.*, 1991; Blackmann, Stein & Vandiver, 1993). Key indicators visible on radiographs consist mainly of orientation of particles and voids and shapes of voids (Vandiver, 1987; Carr, 1990). These have been observed in cross section and normal views of vessel walls and in normal views of bases.

Even though sophisticated analytical techniques such as radiography are used, criteria for recognition of fashioning techniques are still established from qualitative comparisons between archaeological samples and standards (i.e. ethnographic or experimental materials). No quantification of the basic parameters developed in such an empirical approach has been attempted. It is known that X-ray images can be successfully digitized and then subjected to image processing (Vandiver *et al.*, 1991: 203). Precise characterization of some features remaining from ceramic fashioning thus seems potentially possible.

The thickness of the walls of vessels is another indicator of fashioning techniques that has been examined. van der Leeuw (1976) noted differences in thickness of the vessel wall vertically, at joints of rolls and horizontally, where ends of a roll meet. Rye (1981: 60) reported that a skilled potter can infer much of the forming process by feeling subtle variations in thickness and reconstructing the finger and hand movements of the maker. Gradual thinning of the wall thickness from the base to the rims and/or an extreme regularity of wall thickness in horizontal sections have been used to characterize thrown vessels (Picon, 1973; Rye, 1981; Balfet, Fauvet-Berthelot & Monzon, 1983; Vandiver, 1987; Mery, 1991). Given these numerous observations, surprisingly little is known about the significance of this macrofeature. This is because no systematic evaluation of wall thickness with respect to the forming process has been carried out. Also, comparison between a diverse range of samples is difficult because of lack of quantification.

Vandiver *et al.* (1991) outlined the difficulty in making the most of the information provided by X-ray imaging techniques. These techniques (except CT scanning) provide complex images because of the unavoidable superposition of objects and structures resulting from the projection from a volume onto a plane (Raynaud *et al.*, 1989; Vandiver *et al.*, 1991). A drawback is that similar objects in the same image may not be represented within the same range of grey levels. One direct consequence of this problem is that extraction of similar attributes, e.g. voids or mineral inclusions, is difficult when using raw images.

In this paper, we address the issues of visualization of wall thickness and density distribution within sherds. Sherds are exposed to X-rays and the resulting radiograph is digitized using a document scanner. A morphological low-pass filtering operation is used to separate thickness and density information. These images are then calibrated using fundamental X-ray absorption physics supplemented with minimal measurements on the sherds. Such images convey a physical significance and make quantification of several parameters possible.

The proposed methodology is illustrated using experimental material for which the fashioning processes are known. The aim of the examples is to illustrate some of the features that can be enhanced. The use of these features to complement conventional techniques for interpretation of archaeological materials will be dealt with elsewhere.

Image Acquisition

The digital radiographic images used were not obtained by direct digital radiography (Vandiver *et al.*, 1991), but following a two step procedure. First, standard radiographic exposures were obtained on fine-grained industrial Kodak Industrex R film. Sherds of mean thickness between 4 and 10 mm were exposed from 1 to 10 min using a kilovoltage of 50 kV, a tube current of 3 mA and a focal spot-to-film distance (ffd) of 60 cm (for significance of these parameters, see Carr & Riddick, 1990).

The image formed on the film depends on the X-ray intensity received after attenuation by the sample. For a monochromatic radiation, X-ray attenuation through an homogeneous substance is given by Lambert's law:

$$I = I_0 \, e\text{-}\mu\rho E \qquad (1)$$

where I is intensity after attenuation; I_0 is incident intensity; μ is mass absorption coefficient ($cm^2\ g^{-1}$); ρ is gravimetric density ($g\ cm^{-3}$); E is sample thickness (cm). Evidently, local variations of brightness intensity on the radiographic film depend on local variations in composition, gravimetric density and the length of the trajectory of the beam through the object.

To measure correctly variations in wall thickness, the length of the trajectory of the beam through the sherd must be consistent with sherd thickness. This is not the case here because the sherds are curved and a divergent beam was used. The X-ray trajectory will be consistent with sherd thickness if the sample is perpendicular to the line of X-rays at every point, the ideal case being that the sherd's curvature corresponds to the focal distance. Image distortion should be minimised by placing the film as tangential as possible to the sherd's curvature at every point. It is possible to approach these requirements by imaging the sample as close as possible to the X-ray beam axis and by

attaching the film to the convex surface of the sherd with adhesive tape (Carr, 1990; Carr & Riddick, 1990: 43). The tape should be placed only at the edges of the film to avoid any damage to the emulsion when removing the tape.

The second step of the procedure is to digitize the radiographs using a document-scanner. At this stage, the size of pixels can be selected to generate images at an appropriate resolution. Theoretically, very fine grain-size and thin emulsions provide resolutions of at least 200 lines/mm (Drees & Wilding, 1983: 66). However, when imaging sherds, such high resolution may not be justified if there is poor contact between the film and the objects imaged, i.e. pores, particles, etc. (Carr & Riddick, 1990: 41). Therefore, an effective mean resolution of about 50 μm can be expected. This resolution is not a drawback because the pores in which we are interested are larger than 50 μm. Also, for our examples the wall thickness variations indicative of specific fashioning techniques occur over larger distances. With the document-scanner, images were scanned at 300 dpi, which result in pixel length and width of 84 μm. A pixel is an elementary area of an image identified by its location (coordinates) and value. Here, each pixel is allocated a value between 0 and 255 depending on the intensity (or brightness) of the film which reflects the local attenuation of X-rays. This value (or grey level) expresses the successive attenuations the X-ray beam suffers as it encounters elements differing in composition, gravimetric density and thickness, through the whole thickness of the sample. From a ceramological perspective, global attenuation represents the cumulative effect of the thickness of paste, mineral inclusions and voids encountered by X-rays before reaching the film, Hereafter, the image generated after scanning will be known as the raw image.

An inherent limitation to the use of ordinary and high resolution radiographic films is their narrow dynamic range, i.e. their weak capacity to record very different X-ray intensities in a single exposure (Vandiver *et al.*, 1991: 203). Consequently, thickness variations of more than 5 mm cannot be recorded on the radiographs.

Another limitation lies on the film/scanner response. In order to perform correct calibrations by applying Lambert's law, two conditions are required. The first one is to make sure if grey levels on the digital images are always proportional to the transmitted X-ray intensities (i.e. problem of undersaturated or oversaturated range). The second condition is to test if there is a linear proportionality between the image grey-levels and the transmitted X-ray intensities.

In order to estimate the calibration curve of the image grey-levels versus transmitted X-ray intensities, some reference exposures were conducted using a wedge made of quartzite, 0 to 10 mm thick. These tests conducted with the same data acquisition conditions as those used with sherds, show that the film/scanner response is quite linear within a grey-level range from 30 to 255. From these results, it is clear that it is possible to use the grey levels values for deriving thickness and porosity assessments from Lambert's law.

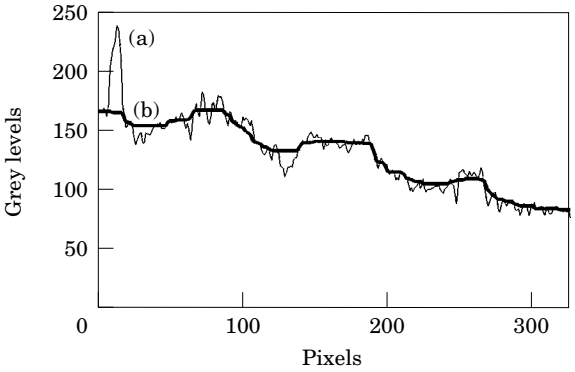

Figure 1. Illustration of thickness derivation. Grey levels for one column of a raw image (a) (—) and its filtered thickness image (b) (—). Narrow peaks and valleys in the raw image are expected to be related to local density heterogeneities, whereas larger-range variations in grey-levels are supposed to correspond to wall thickness variations. Therefore, filtering the raw image results in a thickness image.

Derivation of Thickness Images

It is evident from Lambert's law (equation (1)) that the raw image includes both thickness and porosity information. To use this law to isolate and calibrate the thickness information it is assumed that each sherd is homogeneous in gravimetric density and composition. If this assumption holds the only factor that affects grey level is thickness. Clearly, this assumption is false because temper particles, voids and local variations in paste density create local heterogeneities. As a consequence, raw images are filtered to remove the heterogeneities. Local extrema are suppressed and are converted into values which depend on the grey levels of their neighbouring pixels. The size of the heterogeneities to be suppressed depends on the material studied. The smallest ones can be at the limit of resolution and the largest can be of the order of millimetres.

With this processing, a given number of iterations is applied. In principle, the number of iterations is equal to the radius (expressed in pixels) of the largest heterogeneity assessed by visual examination of the raw image. Filtering is achieved by successive application of two transformations from mathematical morphology known as opening and closing (Serra, 1982). An opening consists of an erosion operation followed by a dilation. In an *erosion*, each pixel is replaced by the *minimum* of its neighbours. In a *dilation*, each pixel is replaced by the *maximum* of its neighbours. Closings are used to remove porous heterogeneities. In a closing of size 1, any pixel with a smaller value than its neighbours will be replaced by a larger value equal to

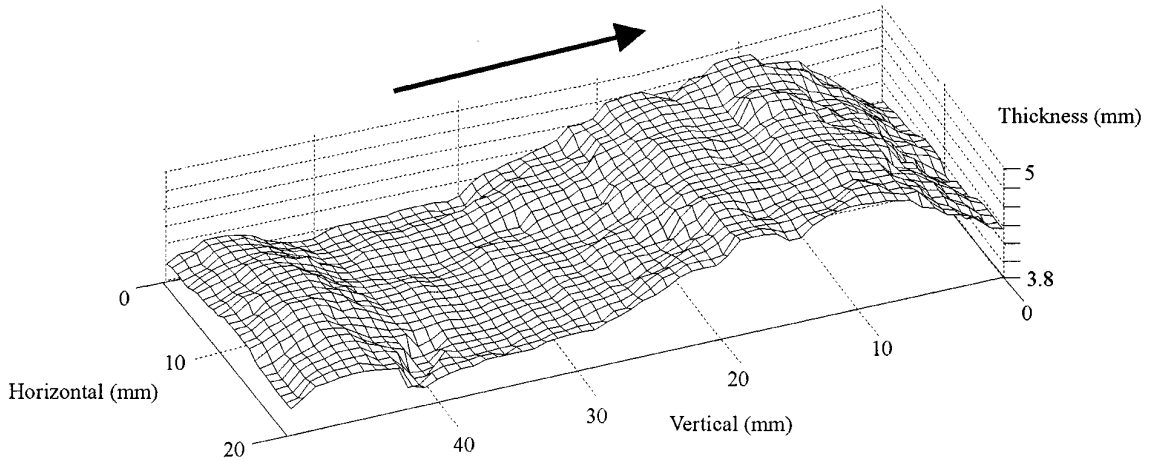

Figure 2. A perspective view of a calibrated thickness image. The arrow above the plot indicates the sherd orientation (from base towards the top).

at least one of its neighbours. Openings are used to remove dense inclusions. In an opening of size 1 any pixel with a larger value than its immediate neighbours will be replaced by a smaller value. Thus, all irregularities of size 1 are removed by an opening followed by a closing (or vice versa). Irregularities of size 2 are removed by 2 openings followed by 2 closings and so on.

The effect of this filtering is illustrated in Figure 1, which shows the modification of grey levels down one column of pixels from a raw image. As expected, local heterogeneities disappear to provide a more global view reflecting variations in wall thickness. In such an image the grey level of each pixel is proportional to sherd thickness following the normal to the pixel surface.

This filtered image can be calibrated to derive actual sherd thicknesses. Filtering is equivalent to replacing the terms μ and ρ in Lambert's law by constant values. Then we can write the following expressions from equation (1):

$$\ln \frac{I_0}{I_i} = kE_i \qquad \text{(a)}$$

$$\ln \frac{I_0}{I_m} = kE_M \qquad \text{(b)}$$

$$\ln \frac{I_0}{I_M} = kE_m \qquad \text{(c)}$$

where I_0 is the incident intensity; E_i is the thickness of the sherd at pixel position i (cm); E_M is the maximum thickness measured on the sherd (cm); E_m is the minimum thickness measured on the sherd (cm); I_M is the maximum grey level in the filtered image I; I_m is the minimum grey level in the filtered image I; I_i is the grey level at point i of filtered image I; and k is the product of constant terms μ (cm^2/g) and ρ (g/cm^3).

Combining (b) and (c) allows derivation of k, and finally, subtraction (b)–(a) gives calibration equation (2)

$$E_i = E_M - \left(\frac{E_M - E_m}{\ln \frac{I_M}{I_m}} \right) \times \ln \frac{I_i}{I_m} \qquad (2)$$

Equation (2) is used to calculate the actual thickness in every point of the image by measuring the thickness of the sherd at the location of two spots corresponding to the largest and the smallest grey levels in the image (or any two known, easily locatable regions).

A perspective view provides a convenient and informative visualization of the thickness map of the sherd under examination (Figure 2). Unlike laser scans of the surface, this is not a strict numerical substitute of the actual object because some geometric properties, e.g. curvature, are not represented. The visualization is a graphic representation of what can be felt by simultaneously touching the internal and external surfaces of the sherd; it expresses quantitatively the thinning and thickening felt with the hand. This quantification provides strict morphometric data to complement conventional qualitative morphologic descriptions. It is not necessarily better than touch because a skilled hand may be very sensitive. It provides a base for more repeatable (precise) and objective description, facilitating comparison of sherds from variable sources and thereby potentially improving the significance of technological descriptions.

There are two sources of possible error associated with this method. Variations in thickness over regions smaller than the number of iterations used for morphological filtering will not be evident in the final image. In cases where identification of such features, e.g. grooves from finger trails on vessel walls, is critical further

processing is required. Important regions could be located visually and processed using fewer iterations of the filter. Such regions could then be re-inserted into the image before calibration. Thickness evaluation may also be affected by local variations in gravimetric density if the integrated density along the X-ray path differs greatly from the mean material density. Large pores within the sherd may result in under-estimation of thickness and dense heterogeneities such as temper particles result in over-estimation. These extrema are usually easy to see in the density image and prior to filtering, could be substituted with the mean density if such detail is required.

Derivation of Porosity and Density Distributions

Porosity distribution is a powerful discriminating attribute for identification of fashioning techniques. Xeroradiography and digital radiography systems have been used for porosity visualization (Vandiver, 1991), but no selective extraction of features has been proposed. Lambert's Law (equation (1)) shows that if thickness information can be extracted it can be used to derive the distribution of gravimetric density in the sherd. The density calibration is achieved with conjugate use of the filtered image and the raw image combined with several simple measurements (equation (3)).

The raw image, J, is used to extract local gravimetric densities ρ_i (equation (d)), whereas an expression of mean gravimetric density ρ is extracted from filtered image I (equation (e)):

$$\rho_i = \frac{\ln \frac{I_0}{J_i}}{\mu_i E_i} \qquad \text{(d)}$$

$$\rho = \frac{\ln \frac{I_0}{I_i}}{\mu E_i} \qquad \text{(e)}$$

where: ρ_i is the gravimetric density in any point i of the image (g cm^{-3}); ρ is the mean gravimetric density measured by immersion (g cm^{-3}); I_0 is the incident intensity; I_i is the grey level in any point i of the filtered image I; J_i is the grey level in any point i of the raw image J; E_i is the thickness of the sherd at pixel position i (cm); μ_i is mass absorption coefficient in any point i of the raw image J (cm^2 g^{-1}); μ is the mean mass absorption coefficient used with the filtered image I (cm^2 g^{-1}).

Subtraction of (d) from (e) allows derivation of the gravimetric density in any point i of the image and can be reduced to an expression where the terms are known. For this we have to replace μ_i actual values in (d) by the mean value μ of (e) because it is not possible to have a local estimation of μ_i. We also need to introduce the expression of E_i given by equation (2). Finally, equation (3) is obtained:

$$\rho_i = \rho \left(1 + \frac{(1-x_m) \times \ln \frac{I_i}{J_i}}{\ln \frac{I_M}{I_m} - (1-x_m) \times \ln \frac{I_i}{I_m}} \right) \qquad (3)$$

where: ρ_i is the gravimetric density in any point i of the image (g cm^{-3}); ρ is the mean gravimetric density measured by immersion (g cm^{-3}); x_m is the ratio of minimum to maximum measured thicknesses; Ii is the grey level in any point i of the filtered image I; J_i is the grey level in any point i of the raw image J; J_M is the maximum grey level in the filtered image I; I_m is the minimum grey level in the filtered image I.

The resulting image represents a virtual object of uniform thickness, in which grey level variations mainly depend on local anomalies related to the gravimetric density of the features contained in the sherd (Figure 3(a)).

It is also possible to make a porosity calibration by assuming that the gravimetric density of the clay solid phase is the maximum density encountered within the sample. With such a porosity calibration, the minimum grey level (black) corresponds to 0 porosity (no void), and the maximum grey level (white) corresponds to 1 porosity (no solid). In the image obtained, the clay paste has a mean grey level whose value corresponds to the mean density measured, whereas pores appear as light regions and heavy inclusions in dark areas (Figure 3(b)).

Very local variations in thickness (which radius in pixels is less than the number of iterations applied) are omitted from the thickness images and appear as part of the density distribution. This arises because of the assumption that density reflects anomalies which do not exhibit thickness variations. A second possible source of error may arise if there are significant deviations from the assumed mean value for the mass absorption coefficient. Raynaud *et al.* (1989: 153) give some values for elements under X-ray energy of 0·080 MeV: iron 0·554 cm^2 g^{-1}, potassium 0·29 cm^2 g^{-1} and silicon 0·203 cm g^{-1}. Therefore, if there are inclusions of large mineral grains whose coefficient differs from the assumed mean (close to silicon) the gravimetric density will be poorly estimated for that location.

Results

The techniques used for forming one part of a vessel are not necessarily an indication of techniques used on another part, *e.g.*, rim versus body (Balfet, 1973; van der Leeuw, 1992). Therefore, the significance of surface and internal features have been discussed only with reference to the zone of the vessel in which they occur (van der Leeuw, 1976: 240; Courty & Roux, 1995).

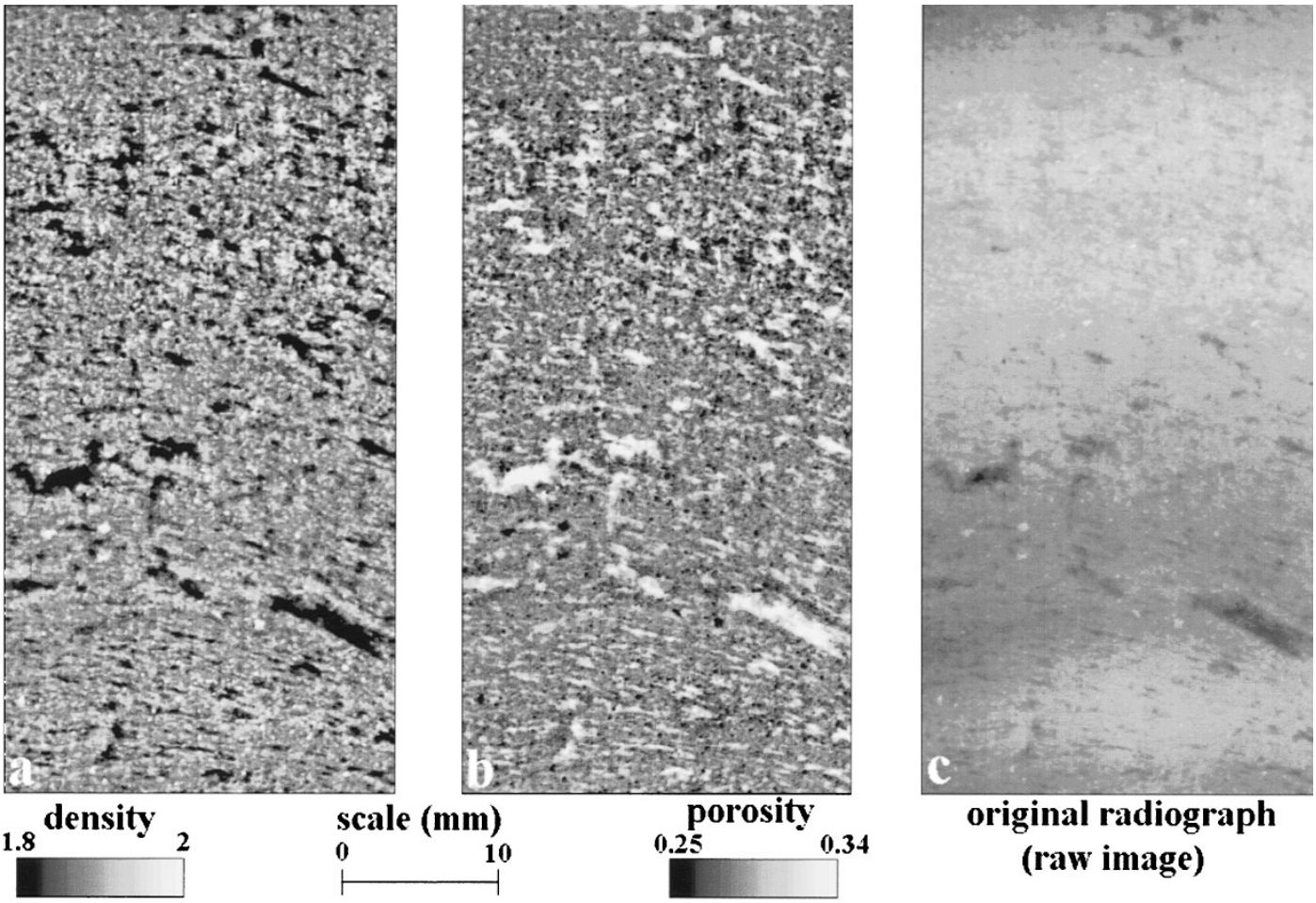

Figure 3. Examples of calibrated (a) density and (b) porosity images for the same sherd whose thickness is shown in Figure 2. (c) Raw image.

Consequently, the results we present only concern the part of vessel which has been investigated. We do not deal here with reconstitution of fashioning methods, i.e. sequences of operations involved in vessel construction, but only with identification of fashioning techniques which can be defined as physical actions on matter (Leroi-Gourhan, 1943).

Experimental Material

The samples used for illustration come from a series of experiments carried out with professional potters in India by V. Roux. Details about experimental procedures are given elsewhere (Roux, 1994; Courty & Roux, 1995). Three fashioning techniques are examined:

(1) coiling with shaping on the wheel,
(2) coiling with thinning and shaping on the wheel,
(3) throwing.

(1) Coiling with shaping on the wheel

The specimen examined came from the upper part of a small restricted vessel. The vessel was fashioned by coiling small rolls of paste of about 10 mm in diameter. The coils were not firmly joined together and the surface was just roughly smoothed on a wheel, without applying the pressure necessary to modify appreciably the geometry of the walls. The sherd submitted to X-ray analysis included a part of the body wall attached to the rim. The part of the sherd investigated was 21×47 mm and was represented in an image 250×560 pixels, i.e. resolution of 84 µm. The calibrated thickness and porosity information is shown in Figure 4.

The thickness of the sherd is between 4·3 and 5·5 mm, i.e. a range of 1·2 mm. Four main horizontal bands which resemble cordons or rounded ridges about 10 mm wide are visible (as indicated by arrows in Figure 4(a)). Their thickness varies by about 1 mm and they are demarcated by shallow grooves. The maximum difference in thickness between the top and the edges of a ridge is around 0·5 to 0·6 mm. These ridges can be interpreted as coils of different thickness which have not been equally levelled by the shaping and finishing operation. Other noticeable details are that there is no general thickness gradient throughout the sherd and narrow coils tend to be thicker than wider ones.

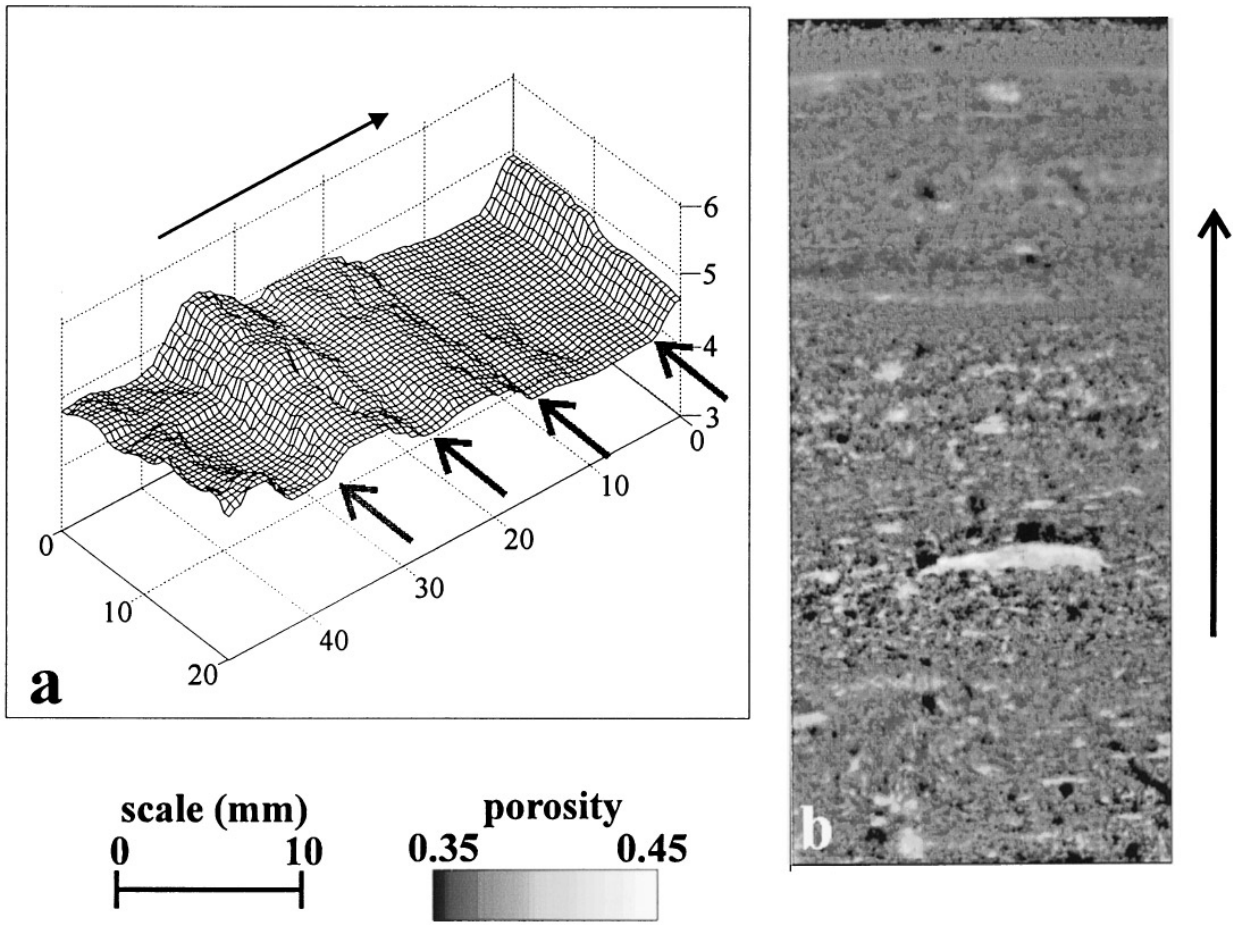

Figure 4. Calibrated data for small restricted vessel formed by coiling with shaping on the wheel. (a) Perspective view of wall-thickness. The arrow above the plot indicates the sherd orientation (from base towards the top). (b) Porosity image of the same specimen. The arrow alongside porosity image indicates the sherd orientation.

The porosity image (Figure 4(b)) shows that porosity is distributed over a wide range of size classes (up to 10 mm long). The porosity for this sherd is between 0·2–0·45, i.e. a range of 0·25 (for display convenience, the porosity range has been restricted to 0·35–0·45 on Figure 4(b)). The pore space is arranged preferentially in the horizontal direction. The anisotropy of smaller pore space is consistent with forces applied during rolling which traps pockets of air inside the coils. The larger elongated vesicles occur at the junction between coils and occasionally as large air pockets inside coils (Carr, 1990: 15). This type of porosity distribution can be explained by the joining of uncompleted coils, low compression stress applied after rolling coils and poor accommodation of successive coils. This matches well with the uneven distribution of thicknesses noted above. Both criteria indicate that no significant forces were employed during the shaping and finishing steps. This example illustrates forming by a skilled potter because of the relatively small range in wall thickness (25%). Rye (1981: 67) observed that the thickest part of some walls built by coiling may be twice as thick as the thinnest parts.

(2) Coiling with thinning and shaping on the wheel

The sherd examined was from the body of another small restricted vessel; neither the base nor the rim were included. Two procedures were used to form the body: coiling with coils about 10 mm in diameter and then thinning the walls thus formed by throwing on a wheel. The part of the sherd investigated was 28·6 × 37 mm and was represented in an image 340 × 440 pixels, i.e. resolution of 84 μm. The thickness of the sherd is between 4·5 and 4·9 mm, i.e. a very small range of 0·4 mm (Figure 5(a)). There is a shallow depression which runs across the sherd about 30 mm down. The thickness gradually increases either side of the depression. Unlike the case of coiling without thinning by throwing, presented above, no clear groove separating the original coils is visible.

The organization of the porosity of this sherd is different from those of the other two cases. The porosity for this sherd is between 0·3–0·38, i.e. a range of only 0·08 (for display convenience, the porosity range have been restricted to 0·365–0·381 on Figure 5(b)). This small range reflects the greater homogeneity of the

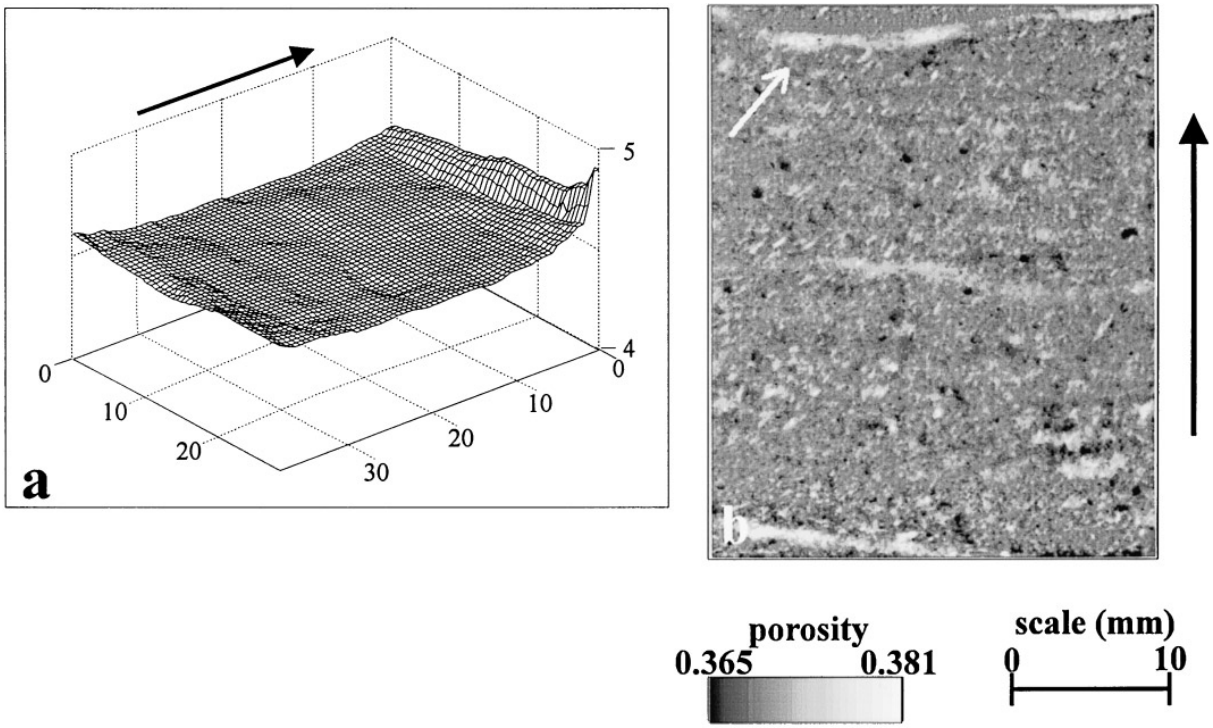

Figure 5. Calibrated data for a small restricted vessel formed by coiling with thinning and shaping on the wheel. (a) Perspective view of thickness image. The arrow above the plot indicates the sherd orientation (from base towards the top). (b) Porosity image of the same specimen. The oblique arrow indicates the preferred orientation of the pores. Notice that some white elongated objects such as those located respectively at the lower, middle and upper parts of the image correspond to superficial grooves. The arrow alongside porosity image indicates the sherd orientation.

gravimetric density in this specimen than the others examined here. There is a mass of small pores (less than 1 mm) whose shape is poorly defined at this resolution (Figure 5(b)). The largest elongate pores show a preferential orientation in a direction strongly inclined to the horizontal ($\sim$45°). This pattern may indicate stretching of pockets of pore space in the initial coils during thinning on the wheel, and has been previously identified by Vandiver (1987: 31). The kind of "trails" located respectively at the lower, middle and upper parts of the image (Figure 5(b)) are superficial grooves, i.e. local thickness variations (whose radius in pixels is less than the number of iterations). They do not appear on the thickness image for the reasons explained above (cf. § derivation of porosity and density distributions).

(3) Throwing

The sherd examined comes from the lower part of the body of a small restricted vessel formed by wheel-throwing a lump of paste. Neither the base nor the rim are represented. The part of the sherd investigated was 25·2 × 27·5 mm and was represented in an image 300 × 328 pixels, i.e. resolution 84 μm. The thickness and porosity information are shown in Figure 6.

Thickness variations occur between 6·5 and 8·3 mm, i.e. a range of 1·8 mm (Figure 6 (a)). There is a regular gradual decrease in thickness from the base to the upside (indicated by the arrow on Figure 6(a)). This general trend is expressed by successive steps of about 8 mm in width which may represent the finger tip width. These steps can be described as asymmetrical ridges with the steeper slope facing up. This morphology was created by different forces being applied to the inside and outside of the walls being thinned by throwing. Pressure was applied to the inside wall by the finger tips held perpendicular to the wall. Simultaneously, the fingers of the other hand were held tightly, but parallel, to the outside wall. Thickness variations imaged here depend both on rilling as defined by Rice (1987: 129), i.e. "rhythmic ridges and grooves that spiral around the vessel walls", and on the regular thinning from the base towards the rims usually associated with clay lifting by throwing (Rye, 1981: 74).

For this sherd, pore sizes are scattered over a small range, and pores larger than 1·5 mm are absent (Figure 6(b)). The porosity for this sherd is between 0·11–0·43, i.e. a range of 0·32 (for display convenience, the porosity range has been restricted to 0·35–0·43 on Figure 6(b)). The largest pores show a preferred orientation slightly slanted to the horizontal. This is an

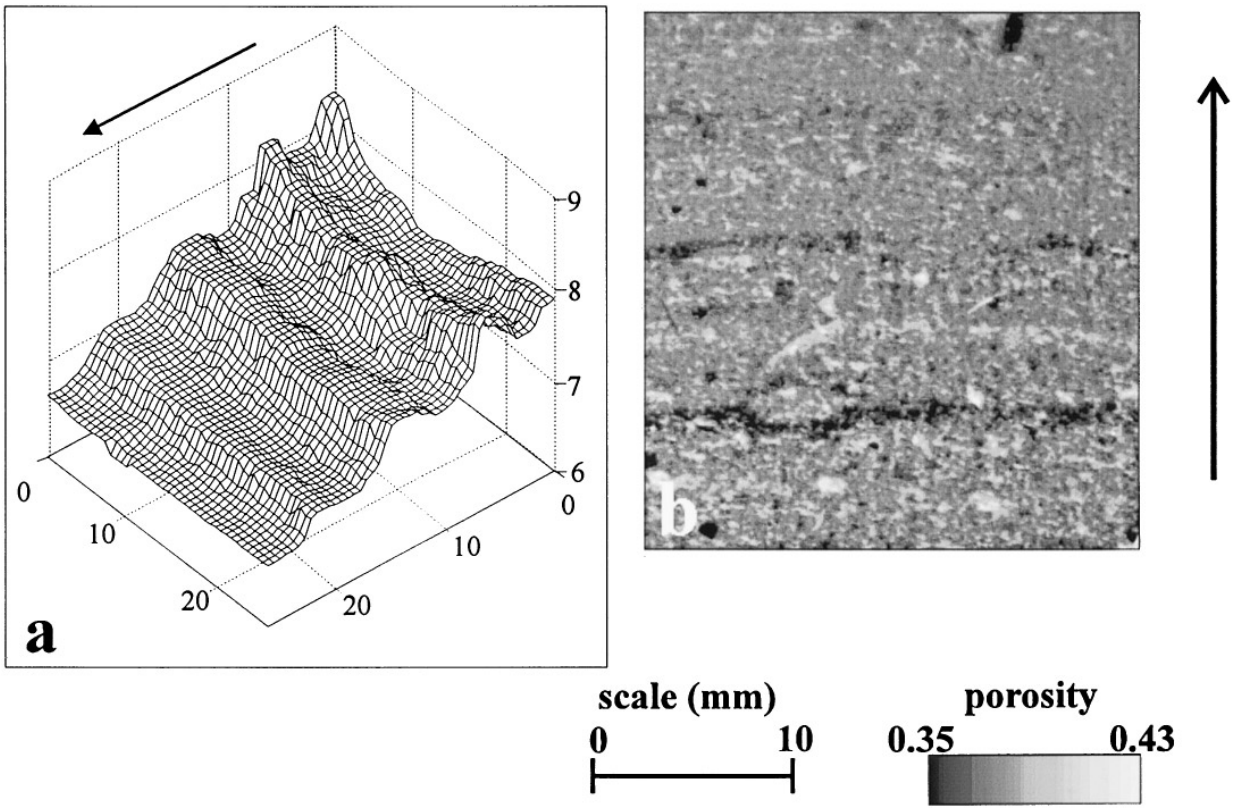

Figure 6. Calibrated data for a small restricted vessel made by throwing. (a) Perspective view of thickness image. The arrow above the plot indicates the sherd orientation (from base towards the top). (b) Porosity image of the same specimen. The arrow alongside porosity image indicates the sherd orientation.

example of the porosity pattern previously found to be specific of thrown vessels by Vandiver (1987: 31).

Conclusions

A methodology based on combination of conventional X-radiography and image processing for visualization of porosity and wall-thickness information has been described and illustrated. Compared to CT scanning for estimation of porosity, our method is calibrated, relatively rapid, easy to perform and low-cost.

Sherds from pots formed with known techniques, namely, coiling with shaping on the wheel, coiling with shaping and thinning on the wheel, and throwing, were used to illustrate the method. Attributes of these specific fashioning techniques were apparent in porosity and thickness visualizations.

Quantification of attributes of wall-thickness and porosity indicative of specific fashioning techniques(s) requires development. There exists a large body of literature describing measurement of binary pore/solid systems using digital images (e.g. Moran, 1994) which can be accessed for this purpose. Also, measurement directly from porosity and thickness images should be explored.

The method proposed here is complementary to conventional techniques for identification of fashioning techniques, e.g. shape analysis, visual examination of surface features and microfabric analysis. It can be performed for some samples representative of recurrent types present in archaeological collections. Identification of fashioning techniques is sometimes oversimplified, i.e. only obvious categories are considered and complex procedures are overlooked. Comparison of data obtained using a range of methodologies may help achieve more sensitive diagnostics of a series of operations.

From an epistemological perspective, a range of experimental examples should be analysed to estimate the relevance of variations in wall thickness to document pottery fashioning techniques. This should include collaborative projects involving both quantification studies and ethnoarchaeological surveys specifically aimed at meticulously documenting such reference data.

Acknowledgements

We thank Valentine Roux, CNRS, ERA 28 for providing experimental material and profitable discussions. We are most grateful to Sabine Renous, Museum National d'Histoire Naturelle for providing access to X-ray equipment and assistance with X-ray images acquisition. Our gratitude is expressed to

Dr M.-C. Girard, INAP-G, who generously made computers available for image processing. The staff at the laboratoire de Science des Sols et Hydrologie is sincerely thanked for supportive critical discussions. CJM is grateful for support from INRA Science du Sol, France and CSIRO Division of Soils, Australia.

References

Balfet, H. (1973). A propos du tour du potier. L'outil et le geste technique. In (CNRS, Ed.) *L'Homme, Hier et Aujourd'hui. Reccueil d'études en hommage à André Leroi-Gourhan*. Paris, Cujas. pp. 109–122.

Balfet, H., Fauvet-Berthelot, M.-F. & Monzon, S. (1983). *Pour la Normalisation de la Description des Poteries*. Paris, Editions du CNRS.

Balfet, H. (1984). Methods for formation and the shape of pottery. In (S. E. van der Leeuw, Ed.) *The Many Dimensions of Pottery. Ceramics in Archaeology and Anthropology*. Amsterdam, Universiteit van Amsterdam. pp. 171–201.

Blackmann, M. J., Stein, G. J. & Vandiver, P. B. (1993). The standardization hypothesis and ceramic mass production: technological, compositional and metric indexes of craft specialization at Tell Leilan, Syria. *American Antiquity* 60–80.

Bordet, P. & Courtois, L. (1967). Etude géologique des céramiques anciennes. Les techniques de fabrication. *Comptes Rendus de l'Académie des Sciences* **265,** 1665–1667.

Carr, C. (1990). Advances in ceramic radiography and analysis: applications and potentials. *Journal of Archaeological Science* **17,** 13–34.

Carr, C. & Riddick, E. (1990). Advances in ceramic radiography and analysis: laboratory methods. *Journal of Archaeological Science* **17,** 35–66.

Courty, M.-A. & Roux, V. (1995). Identification of wheel throwing on the basis of ceramic surface features and microfabrics. *Journal of Archaeological Science* **22,** 17–50.

Drees, L. R. & Wilding, L. P. (1983). Microradiography as a submicroscopic tool. In (E. B. A. Bisdom & J. Ducloux, Eds) *Submicroscopic Studies of Soils*. Developments in Soil Science 12. Oxford: Elsevier. pp. 65–76.

Leroi-Gourhan, A. (1943). *L'Homme et la Matière*. Paris: Albin-Michel.

McGovern, P. E. (1989). Ancient ceramic technology and stylistic change: contrasting studies from southwest and southeast Asia. In (J. Henderson, Ed.) *Scientific Analysis in Archaeology*. Los Angeles, CA: Oxford University Committee for Archaeology, Monograph n°19, and UCLA Institute of Archaeology, Archaeological Research Tools 5. pp. 63–81.

Mery, S. (1991). *Emergence et développement de la production céramique dans la péninsule d'Oman à l'Age du Bronze, en relation avec l'Asie moyenne*. Ph.D. Thesis, Université de Paris, Paris.

Moran, C. J. (1994). Image Processing and Micromorphology. In (A. J. Ringrose-Voase & G. Humphries, Eds) *Soils Micromorphology: Studies in Management and Genesis*. Developments in Soil Science 22. Oxford: Elsevier. pp. 459–482.

Picon, M. (1973). *Introduction à l'etude technique des céramiques sigillées de Lezoux*. Technical Report. Centre de Recherches sur les Techniques Gréco-romaines. Faculté des Sciences Humaines—Dijon. Figlina, 2.

Pierret, A. (1994). Identification des techniques de façonnage: intèrêts des données expérimentales pour l'analyse des microstructures. In (CNRS, Ed.) *Terre Cuite et Société*. Paris: Actes des XIIIèmes Rencontres Internationales d'Archeologie et d'Histoire d'Antibes. Juan les Pins, ADPCA. pp. 75–91.

Raynaud, S., Fabre, D., Mazerolle, F., Geraud, Y. & Latière, H. J. (1989). Analysis of the internal structure of rocks and characterization of mechanical deformation by a non-destructive method: X-ray tomodensitometry. *Tectonophysics* **159,** 149–159.

Rice, P. M. (1987). *Pottery Analysis. A sourcebook*. Chicago, IL: The University of Chicago Press.

Roux, V. (1994). La technique du tournage: definition et reconnaissance par les macrotraces. (In CNRS, Ed.) *Terre Cuite et Société*. Paris: Actes des XIIIèmes Rencontres Internationales d'Archéologie et d'Histoire d'Antibes. Juan les Pins, ADPCA. pp. 45–58.

Rye, O. S. (1977). Pottery manufacturing techniques: X-ray studies. *Archaeometry* **19,** 205–211.

Rye, O. S. (1981). *Pottery Technology. Principles and Reconstruction*. Washington DC: Taraxacum Press.

Shepard, A. O. (1956). *Ceramics for the archaeologist*. Washington DC: Carnegie Institution of Washington.

Serra, J. (1982). *Image Analysis and Mathematical Morphology*. London: Academic Press.

van As, A. (1984). Reconstructing the potter's craft. In (S. E. van der Leeuw, Ed.) *The Many Dimensions of Pottery. Ceramics in Archaeology and Anthropology*. Amsterdam: Universiteit van Amsterdam. pp. 129–164.

van der Leeuw, S. (1976). *Studies in the Technology of Ancient Pottery*. Organization for the Advancement of Pure Research. Amsterdam: Universiteit van Amsterdam.

van der Leeuw, S. (1992). Giving the potter a choice. In (P. Lemonnier, Ed.) *Technological Choices. Transformation in Material Cultures Since the Neolithic*. London: Routledge. pp. 238–288.

Vandiver, P. (1987). Sequential slab construction: a conservative southwest Asiatic tradition ca. 7000–3000 B.C. *Paleorient* **13,** 9–36.

Vandiver, P., Ellingson, W. A., Robinson, T. K., Lobick, J. L. & Séguin, F. K. (1991). New applications of X-radiographic imaging technologies for archaeological ceramics. *Archaeomaterials* **5,** 185–207.

Woods, A. (1985). An introductory note on the use of tangential thin sections for distinguishing between wheel thrown and coil/ring-built vessels. *Bulletin of the Experimental Firing Group* **3,** 100–114.